# Experimental Study of the Particles Influence on the Pyramid Wake within the Turbulent Boundary Layer

Y. T. Cheng, J. Sun[†], P. Chen and W. Y. Chen

*Department of Process Equipment and Control Engineering, Hebei University of Technology, Tianjin, 300130, China*
*National-Local Joint Engineering Laboratory for Energy Conservation in Chemical Process Integration and Resources Utilization, School of Chemical Engineering, Hebei University of Technology, Tianjin, 300130, China*

†*Corresponding Author Email: sunjiao@hebut.edu.cn*

## ABSTRACT

Particle imaging velocimetry (PIV) was used to study the near-field variation of a pyramid rough element in clear water and a liquid–solid boundary layer (thickness: 60 mm). Particles with an average diameter of 355 µm and Stokes number of 4.3 were injected into a 1:1000 mass ratio (solid particles: water) liquid–solid two-phase solution. Experiments were conducted to collect instantaneous velocity field information in the streamwise–normal direction and streamwise–spanwise direction at a Reynolds number of 8350. Then, the average velocity field and turbulence intensity of the rough element wake under single-phase and two-phase conditions were compared, and the morphology and periodicity of the shedding structure were analyzed by using proper orthogonal decomposition (POD) combined with the power spectral density function (PSD). Particles were shown to have no significant impact on the recirculation area in the streamwise–spanwise plane but did result in a reduction of the recirculation zone in the streamwise–normal plane and a 0.2h closer location of the streamline's origin to the obstacle. Along with the weakening of the upwash structure, the particle phase diminishes the velocity gradient along the span direction and turbulence intensity. Structural shedding at the top of the pyramid and near the wall occurred simultaneously, and the same shedding period was maintained. Particularly, in the first two POD modes, the energy of the shedding structure near the wall was higher than that at the obstacle tip, with a maximum energy differential of approximately 6%. The Strouhal number of the shedding structure decreased by particles from 0.217 to 0.209. The concentration distribution and degree of dispersion in the particle-laden flow illustrate different results, with lower statistics in the wake flow field.

Keywords: Turbulence; PIV; POD; Two-phase flow; Particles.

## NOMENCLATURE

| | | | |
|---|---|---|---|
| h | pyramid height | $x$ | streamwise direction |
| *Tur* | turbulent intensity | $y$ | normal height direction |
| u | local velocity | $z$ | spanwise direction |
| $U_\infty$ | free flow velocity | $\zeta$ | apex angle of the pyramid |

## 1. INTRODUCTION

Studying the flow patterns of rough element flow separation and wake evolution is essential for understanding and predicting complex three-dimensional flows. Typically, complex large-scale vortex structures can be observed because of flow separation on rough element surfaces (Deyn *et al.* 2020, Léon *et al.* 2020, Goswami and Hemmati 2021, Wang *et al.* 2021), and the turbulent mixing zone generated in the wake strongly affects heat or mass transfer (Padilla *et al.* 2022, Dezan *et al.* 2020).

Similar phenomena, such as the recirculation zone and continuous shedding of vortices in cube, hemisphere, and cone wakes, occur around various rough elements. Rough elements may induce the formation and shedding of quasiperiodic hairpin vortices. The main mechanism is the response of the potential flow to the base pressure. When the fluid is separated from the rough element, the external fluid causes a decrease in the area between the separated fluid and the wall, causing the streamlines to bend inward (Acarlar and Smith 1987, Léon 2020). To balance the pressure on the curved streamline, the

external fluid spirals inward and generates a centrifugal force field (Wille 1974), which is the reaction of the curvature of the external irrotational flow field that leads to the concentration of the vortex lines and the formation of vortices. The position and morphology of vortex shedding are influenced by the tapered and sharp edges of the 3D rough element. The vortices generated when the fluid encounters the leading edge of the rough element will extend downstream along the sides of the obstacle and may change downstream, leading to a more complex flow (Agui and Andreopoulos 1992). For flow in the turbulent boundary layer, the upstream flow separation position is related to the width of the rough elements. For some bluff bodies, the range of the flow separation area is larger than that of streamlined bodies of the same width, such as airfoils (Martinuzzi and Trop Ea 1993).

The fragmentation of a vortex pair can be described as a transition from a regular vortex structure to turbulence, where the location of vortex fragmentation on the airfoil moves forward with an increasing angle of attack at low incompressible velocities (Donohoe and Bannink 1997). The formation of these vortices can strongly affect the local momentum and energy exchange. Martinuzzi and AbuOmar (2003), and Martinuzzi (2007, 2008) observed the presence of a distinct reflux zone downstream of a pyramid rough element with a well-defined vortex nucleus on the symmetry plane. The position of the vortex core is almost stationary compared with similar structures behind a cube or hemisphere. When the pyramid is submerged inside the boundary layer, alternating vortex shedding pairs may occur downstream (AbuOmar and Martinuzzi 2008).

Periodic fluctuations can be observed in the wake flow (Deyn *et al.* 2020, Martinuzzi 1993). For cones with a top angle of less than 3°, vortex structure shedding can be observed, and the frequency remains constant along the height (Papangelou, 1992). Martinuzzi and Trop Ea (1993) and Martinuzzi 2008) found that periodic shedding structures (top angle C $\leqslant 75°$) appear when the thickness of the boundary layer is similar to the obstacle height, and the periodicity is related to the regular shedding vortices formed around the pyramid. For the measured thin pyramids ($15° < C < 75°$), periodic fluctuations were detected not only in the wake velocity field but also on its surface, that is, periodic shedding vortices started at the surface. The shedding frequency of thin pyramids did not vary significantly along the normal height. Similar conclusions were obtained by Vosper *et al.* (1999), who related the periodicity of the wake to the vortices around the rough element.

The aspect ratio is a crucial factor to consider when studying rough elements because variations in the aspect ratio might influence certain characteristics. According to Saha (2013), a high aspect ratio increases the drag coefficient and Strouhal number, which may be related to the strength of the upwash and downwash. The reattachment of the flow, which may result in the recovery of the base pressure, is also affected by the aspect ratio (Rastan *et al.* 2021). This causes the downwash flow to weaken the mean flow structure. Again, in reaction to variations in the aspect ratio, the downwash and upwash flows also have an impact on the vortices at the tip and base of the rough element (Wang and Zhou 2009). Owing to the influence of the tip-induced downwash, von Kármán-like vortices disappear if the aspect ratio is less than the permitted limit (Sumner *et al.* 2004, Zhang *et al.* 2017).

Many industrial applications, such as boundary layer conveying ashes, pollutants, and fluidized beds, include turbulent flow with scattered particles over walls. In particular, an actual surface always contains various rough elements. The investigation of particle dispersion in turbulent boundary layers with rough elements can advance the knowledge of multiphase flow and ultimately enhance the industrial processes that use these flows (Luo *et al.* 2019). The preferential accumulation mechanism of particles is affected by the vortex created by the roughness, which is crucial for avoiding the deposition of particles on the wall (Marchis *et al.* 2016). Additionally, particles are not easily captured by the wall layer owing to collisions between them and rough elements (Liu *et al.* 2016). In liquid–solid two-phase flow studies, coherent structures in the near-wall region undergo significant momentum exchange when entrained particles are ejected or swept (Righetti and Romano 2004). Research has demonstrated (Crowe *et al.* 1985, Dritselis and Vlachos 2008, Richter and Sullivan 2014) that the particle phase weakens the strength and scale of the vortex when it moves by itself and when it follows the fluid motion. A more intense momentum exchange between large particles and the fluid has a significant effect on the turbulence intensity and Reynolds stress in the near-wall region, while more frequent ejection events occur compared to small particles (Rashidi *et al.* 1990). Moreover, the presence of particles affects the wake structure of the rough element, causing changes in flow characteristics (Gao *et al.* 2021).

Previous studies have been limited by the immature PIV technique, and the study of obstacles is relatively superficial. The periodic characteristics of the turbulence intensity distribution and shedding vortices in the pyramid wake are not well understood. In this study, we measured pyramids within single-phase and liquid–solid boundary layers using the PIV technique to highlight the effect of particles on the investigated wake field. The morphology and period of the shedding structure were analyzed using proper orthogonal decomposition and the power spectral density function. The concentration distribution of the particles in the wake region, which is beneficial for avoiding particle deposition, was also investigated.

## 2. EXPERIMENTAL SETUP

The experimental setup is shown in Fig. 1. The experiments were carried out in a $500 \times 600$ mm2 cross section with a length of 2600 mm. The length, width, and thickness of the experimental plate were 2200 mm, 500 mm, and 15 mm, respectively, and the leading edge of the plate was modified by an ellipse

of 8:1. The flat plate was placed horizontally 120 mm from the bottom of the experimental section. The static pressure gradient of the flow field flowing through the surface of the flat plate was approximately zero by adjusting the trailing edge of the flat plate. To obtain fully developed turbulence and a thick boundary layer, a trip wire with a diameter of 5 mm was placed 100 mm from the leading edge of the flat plate. The base of the pyramid was a square with a side length of 40 mm, and the height of the pyramid was 40 mm (h=40 mm). The boundary layer thickness of the smooth plate was approximately 60 mm, which enabled the pyramid to be entirely immersed. In a thick turbulent boundary layer, the flow pattern around the pyramid is not insensitive to the Reynolds number (Sohankar 2006, Sohankar *et al.* 2017, Bai and Alam 2018). The free flow velocity of the tunnel was adjusted by a frequency converter (U $_\infty$ =0.21 m/s, and the experimental water temperature was 25 ℃. This speed avoids too few periods being captured with slow flow and avoids the inability to capture the flow structure clearly at the acquisition frequency. The density of water was 997 kg/m3, and the kinematic viscosity of water was 0.9055 mm2/s. Polystyrene particles with a diameter of 15 μm are used to trace the flow field. The solid-phase particles were polystyrene of diameter 355 μm, and the particle density was ρp= 1050 kg/m3. The solid particles were injected using an axial flow pump at a speed of 2 L/min. The particles were uniformly dispersed in the flow field at 350 mm from the bottom of the experimental section and at a horizontal distance of 3400 mm from the cone.
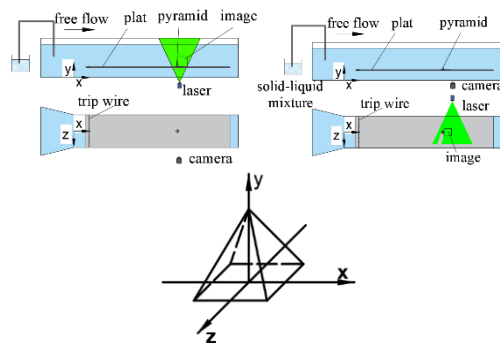


**Fig. 1. Schematic diagram of experimental equipment.**

The PIV system of LaVison Company (Germany) was used for data acquisition; the laser model was LPY700, the maximum frequency of the double pulse laser was 100 Hz, and the maximum energy was 100 mJ. The camera was a 4MX camera (2048 × 2048 pixels) with a maximum sampling frequency of 180 Hz. Double frames and double exposures were adopted in the image field-of-view in the experiment with the center of the pyramid as the sampling position. The image in the x–y plane was approximately 100 × 100, and that in the x–z plane was approximately 115 × 115. Approximately 12000 image pairs were captured at 90 Hz. The displacement between two frames was no less than five pixels in the exposure time. First, the original

image is processed using a Gaussian filter, and then the solid particle phase is extracted using a median filter. Finally, the tracer image of the liquid flow field is obtained by subtracting the particle phase image from the two-phase image. Tracer images were processed using a cross-correlation algorithm with the Davis system. The interrogation window was 32 × 32 pixel, the overlap rate was 50%, and the velocity field contained 128 × 128 velocity vectors. For the flow field images of the liquid and solid phases, the images were first Gaussian filtered before median filtering (Fig. 2). The liquid-phase flow field was obtained by subtracting the solid-phase flow field from the original flow field (Gao *et al.* 2021). The velocity calculated using this technique did not exceed the maximum relative error of 0.05%.



(a)        (b)        (c)
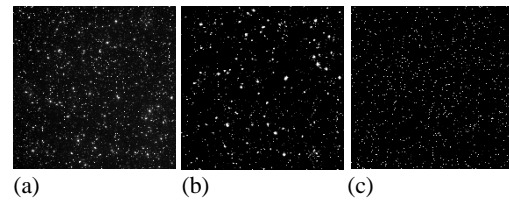
**Fig. 2. Schematic diagram of experimental equipment: (a) original image Gaussian filtering; (b) separating solid image; (c) tracer image.**

## 3. STATISTICS OF FLOW FIELD

### 3.1 Average Velocity

Figure 3 shows the mean streamwise velocity fields of the clear water and particle-laden flow. The size of the blue recirculation zone in Fig. 3(b) is smaller than that in Fig. 3(a), which is obviously caused by the particle phase and is similar to the results behind the hemisphere (Gao *et al.* 2021). Meanwhile, the origin point of streamlines in the recirculation zone moves closer to the cone by approximately 0.2h. However, the normal height of the origin point does not change with the addition of particles and remains at about 0.7h. The fluid velocity above the pyramid is higher than that downstream at the same normal height as the sudden narrowing of the flow cross section. The decrease in the flow velocity might have been caused by the dissipation of the top shedding structure. The velocity field results show that the pyramid clearly disrupts the velocity gradient of the boundary layer.

For the mean flow pattern on the x–z plane, the particle phase did not significantly affect the mean structure, with the center of the reflux zone located at x=0.65h and z=±0.2h at a normal height of y=0.4h. Previous studies have found that the difference in reflux zones along the x–z plane at different normal heights is only represented by the size. The x–z plane located at y=0.4h avoids the excessive influence of the viscous sublayer or a small reflux zone that cannot be clearly observed.

In addition, in single-phase and two-phase situations, the geometry of the negative flow area acts differently. The range of the recirculation zone
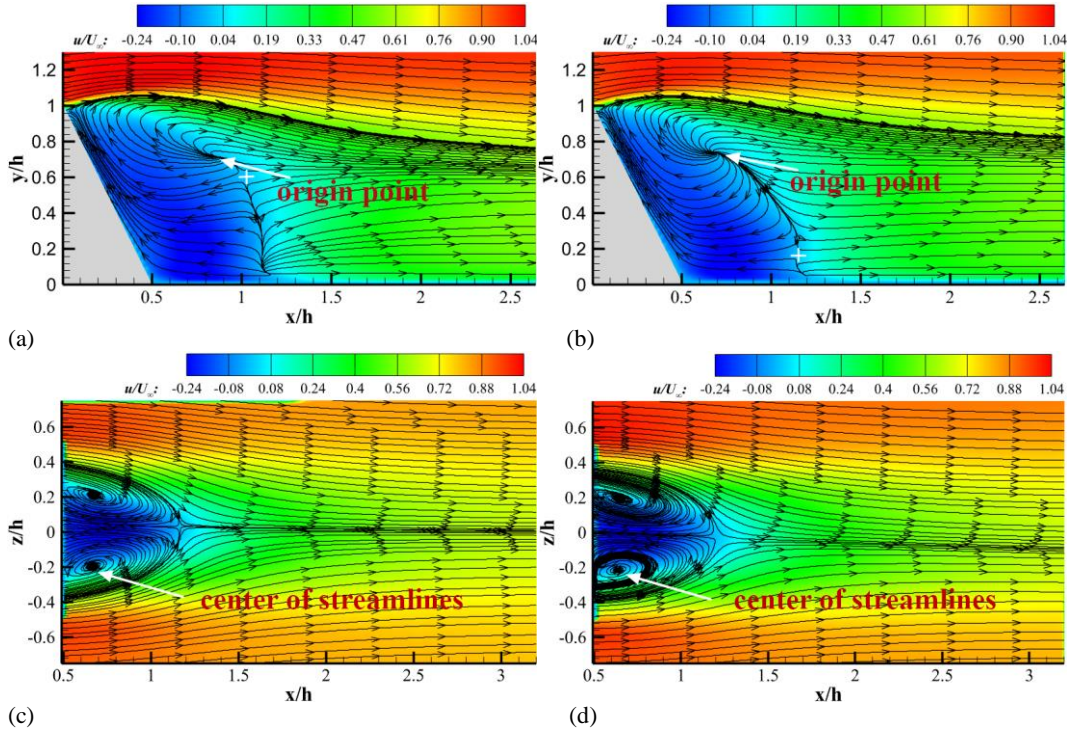
**Fig. 3. Average velocity field of pyramid wake: (a) x-y plane single-phase, z=0; (b) x-y plane two-phase, z=0 (c) x-z plane single-phase, y=0.4h; (d) x-z plane two-phase, y=0.4h.**

increased and then decreased in the single-phase boundary layer as the normal height decreased, whereas it steadily expanded in the two-phase boundary layer. This can be attributed to the different upwash and downwash flows. The downwash flow is only present in the upper portion of the wake in Fig. 3(a), which is comparable to the flow pattern behind a rectangular cylinder submerged in a clear water boundary layer (Wang and Zhou 2009, Hassan *et al*. 2015). The figure's saddle point, denoted by the symbol '+', appears to represent the consequence of interaction between upwash and downwash flows. Owing to the significant reduction in the upwash flow structure caused by the presence of particles, the downwash flow is comparatively enhanced, which causes a shift of the saddle point toward the wall. Because the scale of the base vortices is usually not large, they are easily dissipated by the particles, which is the process of transferring the kinetic energy of the fluid (Boivin *et al*. 1998). The base vortices of the surface-mounted obstacle wake lead to upwash flow (Wang *et al*. 2006), which is weakened because the base vortices are dissipated by the particles. In contrast, the downwash flow shows a stronger tendency, which also causes the saddle point to shift toward the wall.

Compared with the reflux zone on the x–y plane, the photographed x–z plane is closer to the wall, making the viscous force on the fluid stronger than that on the outer fluid, resulting in a less pronounced change in the reflux zone of the mean flow structure.

Figure 4 illustrates the discrepancy in the velocity profiles at different streamwise positions under a particle-laden flow and clear water. Because the
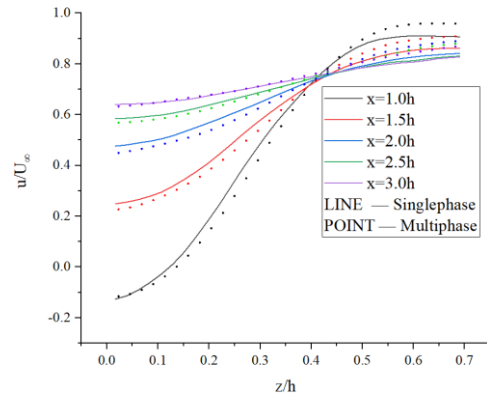


**Fig. 4. Comparison of velocity profiles on the x-z plane at different x/h.**

pyramid wake is symmetrical, half of the velocity profiles are presented to highlight the differences between them (Fig. 4). We observed an intersection of the velocity profile curves at different flow locations, indicating the existence of a fixed z/h value corresponding to the constant velocity of the pyramid wake. When x=1.0h, the velocity profile crosses the recirculation zone, which may be the reason it misses the intersection point. The intersection position is at approximately z=0.44h, which corresponds to a dimensionless velocity of approximately 0.765. When z/h < 0.44, the velocity of the particle-laden flow was lower than that of clear water, and this difference decreased near the intersection point. When z/h > 0.44, it gradually moves away from the symmetrical plane of the pyramid in physical space, and the velocity of the two-phase flow is significantly higher. We believe that the inertia of the particles in the two-phase flow
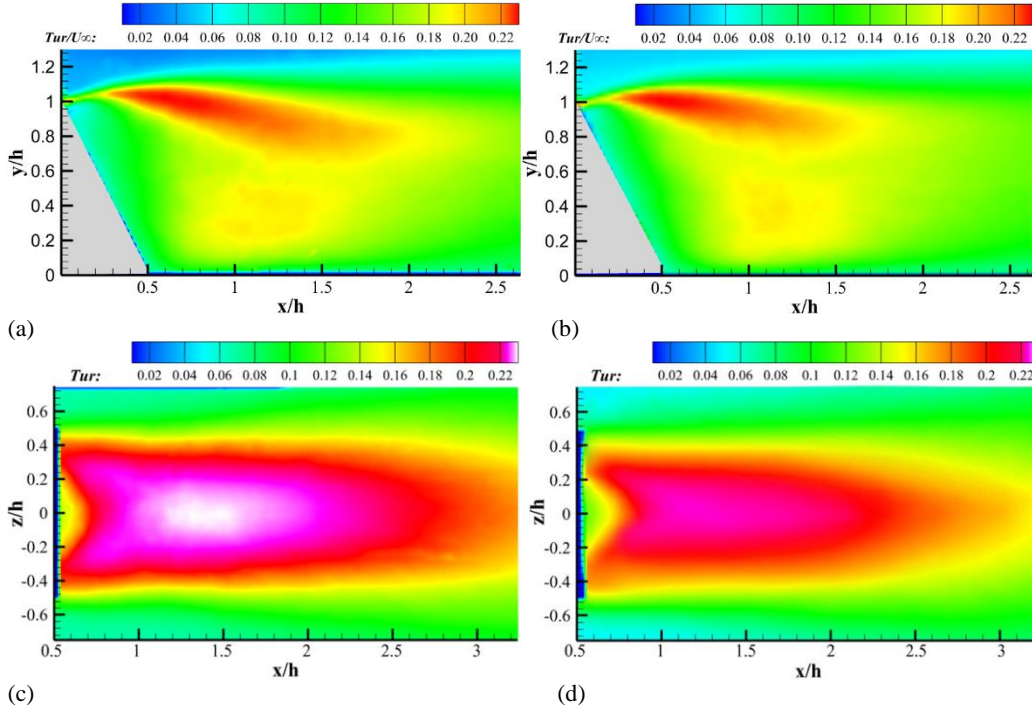
**Fig. 5. Turbulence intensity of the pyramid wake: (a) single-phase flow on the x-y plane, z=0; (b) two-phase flow on the x-y plane, z=0 (c) single-phase flow on the x-z plane, y=0.4h; (d) two-phase flow on the x-z plane, y=0.4h.**

alters the relaxation time of the fluid, leading to a smoother variation in the velocity gradient along the spanwise direction.

## 3.2 Turbulence Intensity

The turbulence intensity is an important criterion for measuring the velocity pulsation, which is usually expressed as the ratio of the pulsation velocity root mean square and time-averaged velocity to the magnitude of pulsation. The turbulence intensity was calculated using Eq. (1), where u' and v' represent the streamwise and wall-normal direction fluctuation velocities, respectively. The spanwise pulsation velocity w' was substituted for v' in Eq. (1) to obtain the turbulence intensity in the streamwise spanwise plane.

$$Tur = \sqrt{\left(\overline{u'^2} + \overline{v'^2}\right)^2 / 2} / U_\infty \qquad (1)$$

The red region trailing downstream from the top of the pyramid is stronger, as shown in Fig. 5(a) and 5(b). The highly turbulent region may be caused by the shedding structure, where the fluid above rushes to the pyramid and is lifted over the top, interacting with the external high-speed fluid to form vortices within the low-speed region and then shedding. The inertia of particles in two-phase flow apparently suppresses the velocity pulsation, leading to a less intense vortex structure than single-phase flow at the same location, which also directly contributes to the reduction of turbulence intensity.

In contrast, another area with higher turbulence intensity appeared near the wall. Previous research has identified what appears to be periodic fluctuations in the x–z plane wake, which is different

from the vortex shedding at the top of the pyramid. Typically, the main vorticity of the shedding structure on the horizontal plane should be provided by the x- and z-directions; however, variations in the turbulence intensity can also be observed on the x–y plane. The presence of a rough element taper, which tilts the rotation axis of the shedding structure, leads to a non-negligible component of its vorticity in the y-direction.

For the turbulence intensity cloud on the x–z plane (Tur > 0.14 can be considered as a high turbulence intensity, as shown in Fig. 5(c) and 5 (d)), the high turbulence intensity region almost coincides with the region bounded by z/h=±0.44 in Fig. 3(c) and 3(d). This is the exact intersection of the velocity profiles shown in Fig. 4. The shedding structure contributes to a significantly higher velocity pulsation than that at the sides of the pyramid. In agreement with the comparison of Fig. 5(a) and 5(b), the particles suppressed the velocity pulsation in the wake region, leading to a decrease in the turbulence intensity.

Furthermore, some changes in the flow structure may be linked to the reduction in turbulence intensity. The position in red with the highest turbulence intensity, indicated by Fig. 5(a) and 5(b), is close to x=0.5h. The coiled-up vortices in the separated shear layer may start shedding at this location, carrying more initial energy as they move downstream. The particle phase clearly suppresses the upwashing flow, as shown in Fig. 3(a) and 3(b), which results in a downwash-dominated particle-laden flow. These findings concur with those shown in Fig. 5(c) and 5(d), which shows that the presence of particles greatly reduces the turbulence intensity on the x–z plane near the wall. We believe that the shear layer in the pyramid wake performs the same function as

the shear layer behind some other obstacles, which makes a significant contribution to turbulence intensity (Hayakawa *et al*. 1984, Kirkil and Constantinescu 2012). The presence of particles reduces the turbulence intensity on both the x–y and x–z planes. This phenomenon is consistent with certain claims that particles weaken the large-scale shear layer structure (Squires and Eaton 1990, Hetsroni 1989)

## 4.    PROPER    ORTHOGONAL DECOMPOSITION

The proper orthogonal decomposition (POD) is considered as an effective technique to study fluid mechanics. The main energy structure indicates that flow patterns can be extracted and represented as flow information with different energy levels. The average velocity field was considered as the 0th mode of the POD, and the rest of the snapshots were ordered by the energy scale (Schmidt and Colonius 2020). Each order of modes constitutes a fundamental flow structure, and their contribution to the entire flow field is investigated by analyzing each mode. The results of 6000 flow field snapshots can occupy the complete energy of the flow field under single-phase and two-phase conditions (Fig. 6). The sample size, which roughly equates to 67 shedding cycles, was adequate for convergent POD analysis.
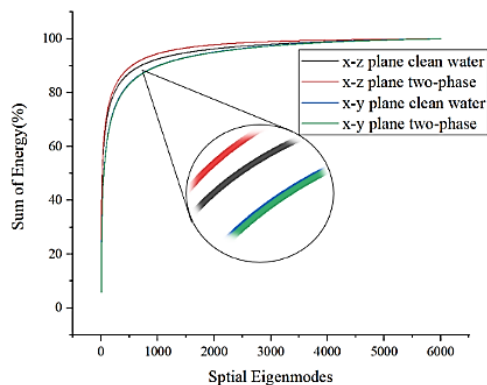
**Fig. 6. Correlation between the number of snapshots and the total energy share of the flow field.**

Figure 7 shows the energy share of the first 20 modes for each operating condition. The energy proportion of the first two modes of POD results on the x–z plane is significantly higher than that on the x–y plane. The first six orders of the POD modes occupy most of the flow-field energy and contribute substantially to the flow structure. The particles increase the first-mode energy on the respective shooting planes.

The inertia of the particles dissipates small-scale turbulent structures, leading to an increase in the energy share of the dominant structure to the entire flow field. This effect is more evident on the x–z plane, where the two-phase case accounts for a significantly higher energy per order than the single-phase case in the structure decomposed by the 3rd–7th modes.
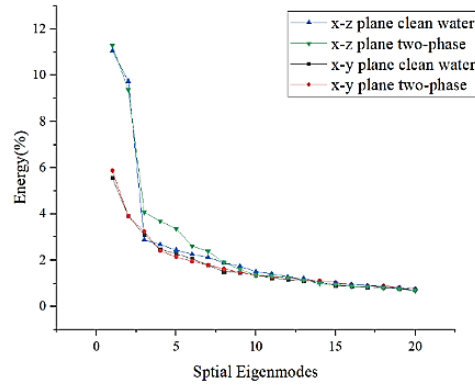
**Fig. 7. Energy share of the first 20 orders of POD results.**

The pyramid wake structures are compared for the two operating conditions based on the streamwise and normal velocities, respectively, as shown in Fig. 8 and 9. The lower modes represent more energetic structures in the flow field, which are typically large-scale flows in the flow field. By comparing the POD results for the single-phase and two-phase conditions, it can be seen that the pyramid wakes are very similar. The presence of the particle phase does not affect the basic structure of wake shedding but is more obvious in the magnitude of the energy. The first two modes are larger shear layer structures, and the particles shift their positions slightly backward. In the first mode, the flow structure in the two-phase results was slightly higher than that in the single-phase results. Comparing Fig. 8(a) and 8(b), it can be seen that in the 3rd–6th POD modes, a teardrop-like structure trailing downstream forms at the tip of the pyramid and evolves along the downstream, which proves that the fluid squeezes the low-speed region after bypassing the obstacle. The resulting apparent periodic vortex structure is seen to be shed from the obstacle tip, and the two-phase case seems to capture more structures in the same window, which is particularly evident in mode 5. The shedding structure becomes progressively larger along the flow direction, which indicates that a diffusion process occurs after vortex shedding, and the presence of particles makes the shape more regular. The effect caused by base shedding can be clearly seen in the 6th mode of Fig. 8(c) and 8(d), where the shedding of the pyramid at the top and bottom can be considered to occur simultaneously. The top structure, away from the obstacle in the flow direction, gradually approaches the wall owing to the presence of particles, which is related to the flow structure in Fig. 3(b), where the downwash dominates the flow. This appears to be more obvious in the second and third modes, as the shedding structure falls toward the wall as a result of the weakening of the upwash.

The POD results for the single-phase and two-phase conditions on the x–z plane are shown in Fig. 9. According to Konstantinidis *et al*. (2007), the mirrored symmetry of the POD vorticity field with respect to the centerline represents a symmetric vorticity field. The first and second modes are plainly seen to accrue alternately, indicating that the first two
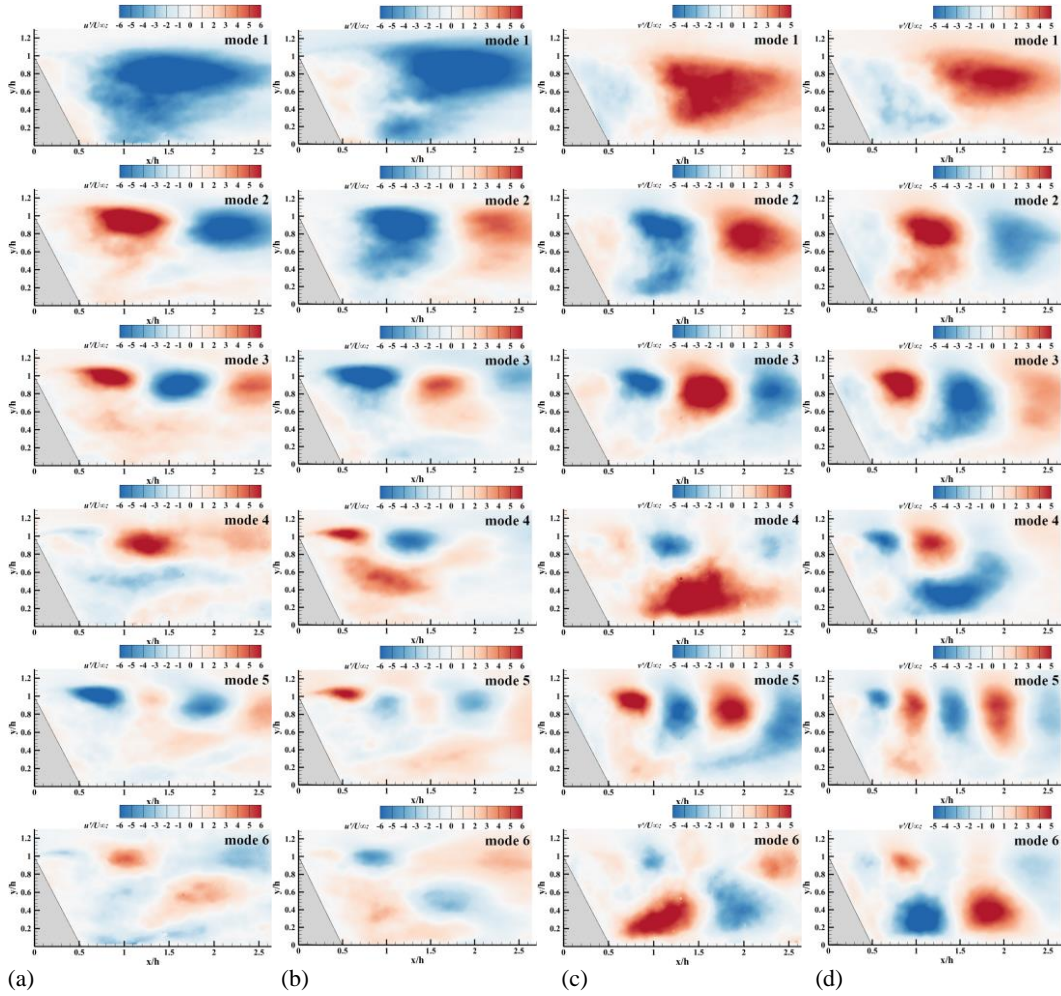
**Fig. 8. POD results for the first 6 modes on the x-y plane: (a) Streamwise fluctuation velocity in single-phase (b) Streamwise fluctuation velocity in two-phase (c) Normal fluctuation velocity in single-phase (d) Normal fluctuation velocity in two-phase.**
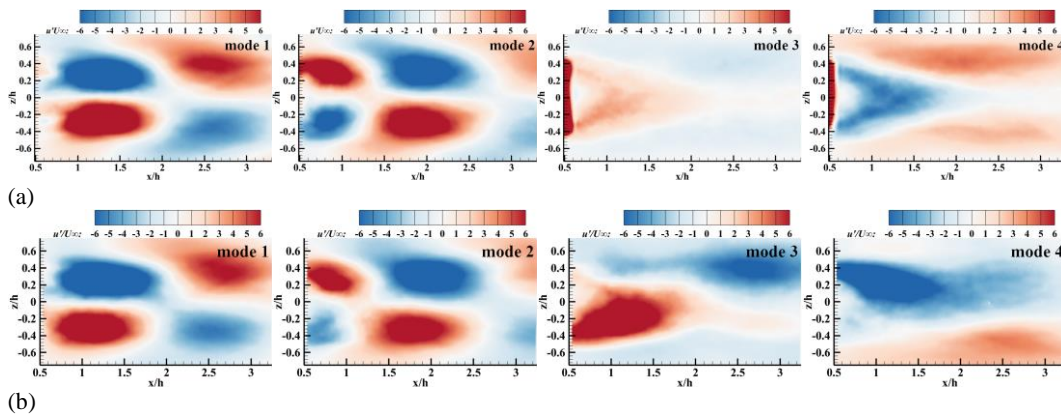


**Fig. 9. POD results for the first 4 orders on the x-z plane: (a) Single-phase; (b) Two-phase.**

modes represent the alternative shedding of the wake. However, the result presented by the POD mode is not a single flow frequency, resulting in the 3rd and 4th modes exhibiting shear layers. Particles appear to break the symmetry of the shear layer in the POD mode. This is comparable to the weak alternative behavior of the rectangular cylinder wake that the authors attributed to the impact of downwash (Yousif and Lim 2021). We agree with them because

the downwash structure of the pyramid wake evolves as a result of particle addition.

## 5. POWER SPECTRAL DENSITY FUNCTION

The periodicity patterns of the different shedding structures at the top and base of the pyramid wake

were analyzed using a power spectral density (PSD) function. The PSD method defines the distribution of the signal with frequency, and a series of specific locations can be selected to determine the intrinsic frequency of the shedding structure and energy change at different locations. To effectively prevent spectral leakage, we utilized the PSD computations of the pwelch function of the MATLAB software and its corresponding Hanning window. The input frequency was 90 Hz, which was the same as the PIV acquisition frequency, with a signal overlap of 50% for each segment. For convergent PSD results, a sample size of more than 3000 was sufficient.

The information of several flow directions of 0.5h, 1.0h, 1.5h, 2.0h, 2.5h after the pyramid with normal height y=0.7h is extracted (Fig. 10). The structure within the turbulent boundary layer evolves mainly in the normal direction, which may lead to the detection of multiple shedding frequencies in the x-y plane. The power of the shedding structure showed a trend of increasing and then decreasing under various working conditions. The extreme value of the detected point on the x–y plane occurs at x=1.5h, while it occurs at x=2.0h on the x–z plane. This indicates that the location where the periodic shedding on the x–z plane begins to dissipate much further from the obstacle. A comparison of Fig. 10(a)
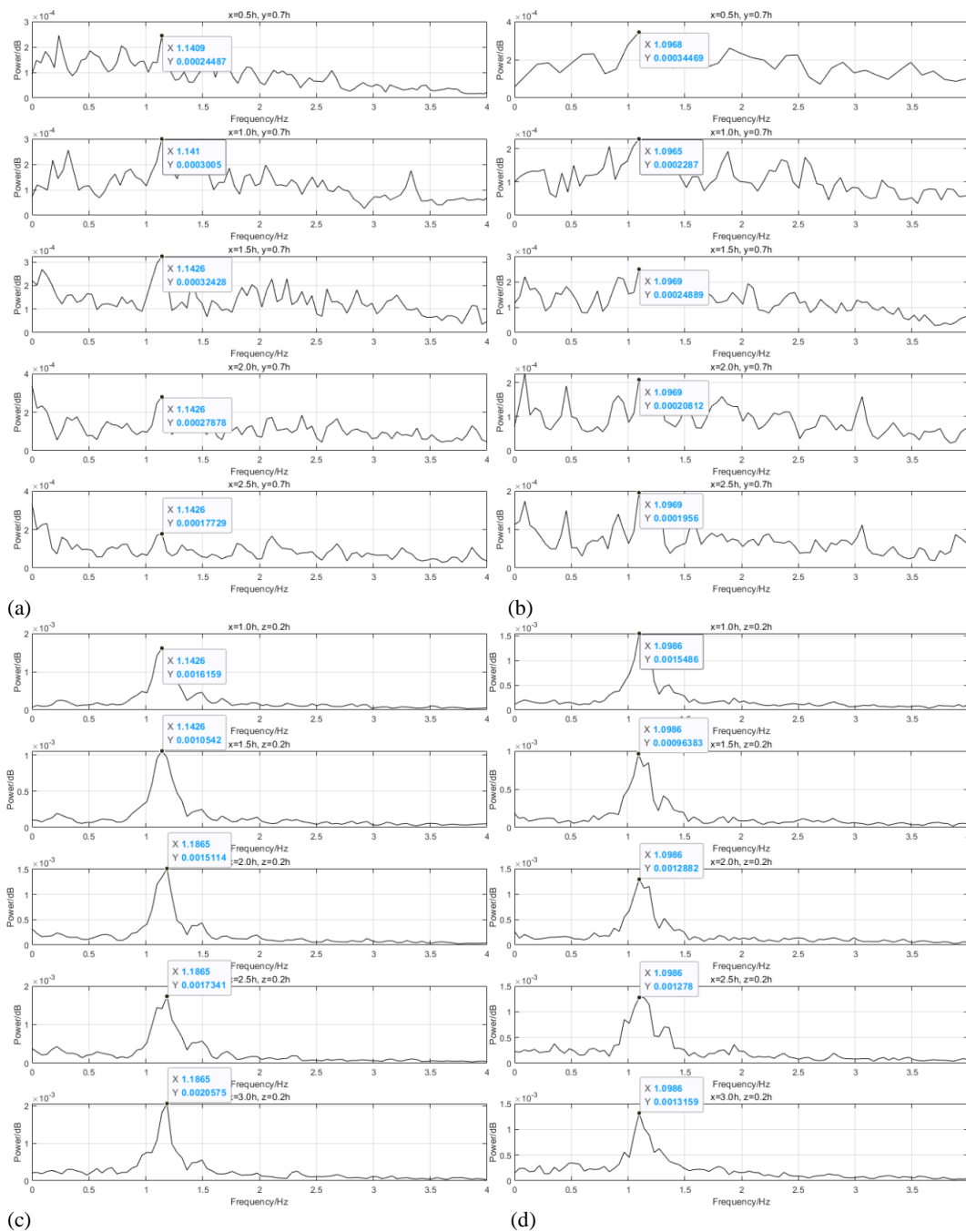


**Fig. 10. Power spectral density function plot, single-phase flow on the x-y plane, (b) two-phase flow on the x-y plane, (c) single-phase flow on the x-z plane, (d) two-phase flow on the x-z plane.**

and 10(c) or Fig. 10(b) and 10(d) shows that the vortices at the tip and base have the same period, proving that the periodic structures at both sites are closely associated. According to Hosseini *et al.* (2016), this is a large-scale structure shedding from the pyramid, and the PSD results in Fig. 10 demonstrate that the inclusion of the particles does not compromise their integrity. The vortex shedding period was approximately 1.14 Hz under single-phase conditions, which corresponds to a Strohal number of 0.217. The dimensionless frequency for an identical structure under the two-phase operating conditions was 0.209. The modulation of the fluid by particles seems to suppress the frequency of vortex shedding. The presence of solid inertia causes the energy to maintain the flow dynamics partially occupied by the particles.

The information of the extracted flow position on the x–z plane is 1.0h, 1.5h, 2.0h, 2.5h, 3.0h with z=0.2h. The energy of the periodically constant vortex shedding at the same flow position was reduced under two-phase conditions. As shown in Fig. 10, the plane of normal height y=0.4h considerably reflects the periodicity of the shedding structure. The spectrograms express apparent periodicity, and almost no noise can be detected in the results.

In general, different vortex shedding is detected on the streamwise-normal and streamwise-spanwise planes. Their periods are constant, indicating that the pyramid wake structures are highly correlated. We believe that the top shedding structure is a response of the high-velocity fluid above the pyramid to the low-pressure region on the leeward side. In contrast, the flow separation on the pyramid surface leads to vortex shedding on the streamwise–spanwise plane, which is similar to the Carmen vortex (Wang *et al.* 2020, Jiang 2021). Furthermore, the vortex shedding energy on the x–z plane is significantly higher than that on the x–y plane for the same operating conditions. Generally, the energy of a vortex structure is positively related to the scale. The area of obstruction to the flow increases near the wall, which leads to the formation of a larger-scale vortex structure.

## 6. CONCENTRATION DISTRIBUTION OF PARTICLES

To investigate the effect of the roughness element on the concentration distribution of particles in the liquid–solid boundary layer, we divided the photographed flow field into two parts to account for the variation in particle concentration (Fig. 11). The dividing line almost reached the boundary layer height. The statistics were selected based on 2000 snapshots of the flow field, which contained more than 20 shedding periods. Figure 12 illustrates a histogram of the particle concentration distribution in the region, which indicates the degree of particle dispersion. The slender distribution indicates a smaller standard deviation, which suggests a lower degree of particle dispersion. The wide concentration distribution in the flow field above the obstacle indicates that the dispersion of the particles in the region is higher

than that in the wake. We believe that the shear layer formed by vortex shedding restricts the particle motion and reduces randomness.
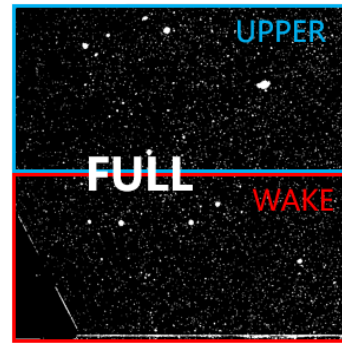


**Fig. 11. Schematic illustration of recording image partitions.**

Figure 13 shows how the particle dispersion varies in time, with a significantly lower dispersion in the wake region. The investigation found significant discrepancies of the concentrations among different flow field regions, and the statistics show that the concentration in the wake field is lower than that in the upper flow field. This suggests that the presence of an obstacle can effectively prevent particles from depositing on the wall.
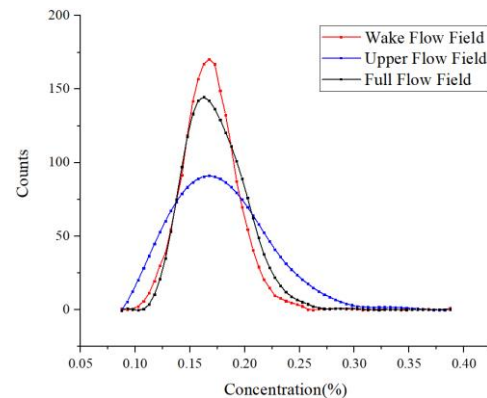


**Fig. 12. Histogram of particle concentration distribution.**
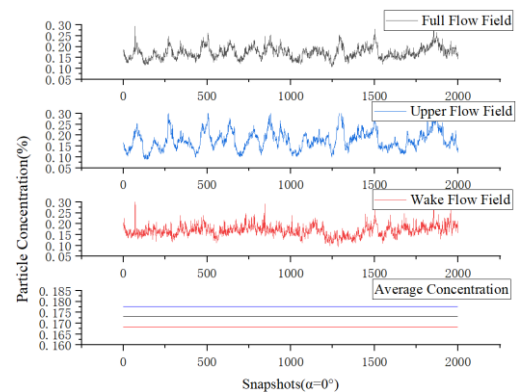


**Fig. 13. Variation of particle concentration with collected samples.**

Typically, the particles in the wake are carried into the region following the formation of the vortex, but inertia causes the particles to not follow the fluid completely. Some particles with longer relaxation times have a greater opportunity to escape from the confines of the vortex, which results in only a part of the particles being carried into the wake-shedding region. This also directly contributes to the fact that the wake concentration is lower than that of the upper flow field.

## 7. CONCLUSION

In this study, the discrepancy of the near-wake field behind pyramid rough elements in clear water and liquid–solid boundary layers was investigated using PIV, and the variation in statistics was analyzed. The POD and PSD methods were used to study the morphology and period of the pyramidal wake. The concentration characteristics of the particles in the flow field region were determined, and the following conclusions were obtained:

(1)    The addition of the particulate phase reduces the size of the reflux zone in the flow normal plane and the location of the flow origin point closer to the pyramid; however, no significant effect on the mean flow structure appears on the flow–spanwise plane. The particles reduce the velocity gradient along the spanwise direction, making the velocity profile gentler. The velocity pulsation was suppressed in the pyramid wake, leading to a decrease in the turbulence intensity. The two-phase flow also exhibits a downwash-dominated flow because the upwash structure is significantly weakened in the flow field.

(2)    POD results revealed that vortex shedding occurred simultaneously at the top and bottom of the pyramid. Tip shedding is clearly visible on the x–y plane, where the weakening of the upwash affects the vortex morphology. Alternating shedding was observed on the x–z plane in all cases. The energy of the first few orders of the POD results also increased because of the dissipation of small-scale structures by particles.

(3)    The PSD results clearly show the periodicity of the shedding structure, and the periods of the top and bottom shedding were found to be equivalent. The energy of the bottom shedding is higher than that of the top shedding, which is attributed to the increase in the vortex scale. The particles apparently suppress the shedding structure period.

(4)    The dispersion and concentration distributions of particles in the wake field were lower than those in the upper flow field. Inertia leads to only a part of the particles being carried into the wake. This significantly contributes to the study of particle deposition avoidance.

## REFERENCES

Acarlar, M. S. and C. R. Smith (1987). A study of hairpin vortices in a laminar boundary layer. Part 2. Hairpin vortices generated by fluid injection. *Journal of Fluid Mechanics* 175, 43-83.

AbuOmar, M. M. and R. J. Martinuzzi (2008). Vortical structures around a surface-mounted pyramid in a thin boundary layer. *Journal of Wind Engineering and Industrial Aerodynamics* 96(6-7), 769-778.

Agui, J. H. and J. Andreopoulos (1992) Experimental investigation of a three-dimensional boundary layer flow in the vicinity of an upright wall mounted cylinder. *Trans Asme* 114(4), 566-576

Bai, H. and M. M. Alam (2018). Dependence of square cylinder wake on Reynolds number. *Physics of Fluids* 30(1), 015102.

Boivin, M., O. Simonin and K. D. Squires (1998). Direct numerical simulation of turbulence modulation by particles in isotropic turbulence. *Journal of Fluid Mechanics* 375, 235-263.

Crowe, C. T., R. A. Gore and T. R. Troutt (1985). Particle dispersion by coherent structures in free shear flows. *Particulate Science and Technology 3*(3-4), 149-158.

De Marchis, M., B. Milici and G. Sardina and E. Napoli (2016). Interaction between turbulent structures and particles in roughened channel. *International Journal of Multiphase Flow* 78, 117-131.

Dezan, D. J., A. D. Rocha and L. O. Salviano (2020). Thermo-hydraulic optimization of a solar air heater duct with non-periodic rows of rectangular winglet pairs. *Solar Energy* 207, 1172-1190.

Deyn, L. H., P. Forooghi, B. Frohnapfel, P. Schlatter, A. Hanifi and D. S. Henningson (2020). Direct numerical simulations of bypass transition over distributed roughness. *AIAA Journal* 58(2), 702-711.

Donohoe, S. R. and W. J. Bannink (1997). Surface reflective visualizations of shock-wave/vortex interactions above a delta wing. *AIAA Journal* 35(10), 1568-1573.

Dritselis, C. D. and N. S. Vlachos (2008). Numerical study of educed coherent structures in the near-wall region of a particle-laden channel flow. *Physics of Fluids* 20(5), 055103.

Gao, T. D., J. Sun, W. Y. Chen, Y. Fan and Y. T. Zhang (2021). Experimental investigation on the effect of particles on large scale vortices of an isolated hemispherical roughness element. *Physics of Fluids* 33(6), 063308.

Goswami, S. and A. Hemmati (2021). Evolution of

turbulent pipe flow recovery over a square bar roughness element at a range of Reynolds numbers. *Physics of Fluids* 33(3), 035113.

Hayakawa, K., A. J. Smits and S. M. Bogdonoff (1984). Turbulence measurements in a compressible reattaching shear layer. *AIAA Journal* 22(7), 889-895.

Hetsroni, G. (1989). Particles-turbulence interaction. *International Journal of Multiphase Flow* 15(5), 735-746.

El Hassan, M., J. Bourgeois and R. Martinuzzi (2015). Boundary layer effect on the vortex shedding of wall-mounted rectangular cylinder. *Experiments in Fluids* 56(2), 1-19.

Hosseini, Z., R. J. Martinuzzi and B. R. Noack (2016). Modal energy flow analysis of a highly modulated wake behind a wall-mounted pyramid. *Journal of Fluid Mechanics* 798, 717-750.

Jiang, H. (2021). Formation mechanism of a secondary vortex street in a cylinder wake. *Journal of Fluid Mechanics* 915.

Kirkil, G. and G. Constantinescu (2012). A numerical study of the laminar necklace vortex system and its effect on the wake for a circular cylinder. *Physics of Fluids* 24(7), 073602.

Konstantinidis, E., S. Balabani and M. Yianneskis (2007). Bimodal vortex shedding in a perturbed cylinder wake. *Physics of Fluids* 19(1), 011701.

Léon, O., P. Reulet and F. Chedevergne (2020). Aerodynamic and heat transfer effects of distributed hemispherical roughness elements inducing step changes in a turbulent boundary layer. *International Journal of Heat and Fluid Flow* 85, 108672.

Liu, X., H. Zhao, K. Luo and J. Fan (2016). Direct numerical simulation of turbulent boundary layer over hemispherical rough walls. *International Journal of Multiphase Flow* 83, 128-141.

Luo, K., Q. Dai, X. Liu and J. Fan (2019). Effects of wall roughness on particle dynamics in a spatially developing turbulent boundary layer. *International Journal of Multiphase Flow* 111, 140-157.

Martinuzzi, R. and C. Trop Ea (1993). The flow around surface-mounted prismatic obstacles placed in a fully developed channel flow. *Journal of Fluids Engineer* 115(1), 85-92.

Martinuzzi, R. J. and M. AbuOmar (2003). Study of the flow around surface-mounted pyramids. *Experiments in Fluids* 34(3), 379-389.

Martinuzzi, R., M. Abuomar and E. Savory (2007). Scaling of the wall pressure field around surface-mounted pyramids and other bluff bodies. *Journal of Fluids Engineering* 129(9), 1147.

Martinuzzi, R. J. (2008). Dual vortex structure shedding from low aspect ratio, surface-mounted pyramids. *Journal of Turbulence* (9), N28.

Padilla, M., I., F. Miró Miró and F. Pinna (2022). Influence of High-Temperature Effects on the Stability of the Wake Behind an Isolated Roughness Element in Hypersonic Flow. In *IUTAM Laminar-Turbulent Transition* 631-642

Papangelou, A. (1992). Vortex shedding from slender cones at low Reynolds numbers. *Journal of Fluid Mechanics* 242, 299-321.

Rashidi, M., G. Hetsroni and S. Banerjee (1990). Particle-turbulence interaction in a boundary layer. *International Journal of Multiphase Flow* 16(6), 935-949.

Rastan, M. R., H. Shahbazi and A. Sohankar, M. M. Alam and Y. Zhou (2021). The wake of a wall-mounted rectangular cylinder: Cross-sectional aspect ratio effect. *Journal of Wind Engineering and Industrial Aerodynamics* 213, 104615.

Richter, D. H. and P. P. Sullivan (2014). Modification of near-wall coherent structures by inertial particles. *Physics of Fluids* 26(10), 103304.

Righetti, M. and G. P. Romano (2004). Particle–fluid interactions in a plane near-wall turbulent flow. *Journal of Fluid Mechanics 505*, 93-121.

Saha, A. K. (2013). Unsteady flow past a finite square cylinder mounted on a wall at low Reynolds number. *Computers & Fluids* 88, 599-615.

Schmidt, O. T. and T. Colonius (2020). Guide to spectral proper orthogonal decomposition. *AIAA Journal* 58(3), 1023-1033.

Sohankar, A. (2006). Flow over a bluff body from moderate to high Reynolds numbers using large eddy simulation. *Computers & Fluids* 35(10), 1154-1168.

Sohankar, A., M. K. Esfeh, H. Pourjafari, M. M. Alam and L. Wang (2017). Features of the flow over a finite length square prism on a wall at various incidence angles. *Wind & Structures* 26(5), 317-329.

Squires, K. D. and J. K. Eaton (1990). Particle response and turbulence modification in isotropic turbulence. *Physics of Fluids A: Fluid Dynamics* 2(7), 1191-1203.

Sumner, D., J. L. Heseltine and O. J. P. Dansereau (2004). Wake structure of a finite circular cylinder of small aspect ratio. *Experiments in Fluids* 37(5), 720-730.

Vosper, S. B., I. P. Castro and W. H. Snyder and S. D. Mobbs (1999). Experimental studies of strongly stratified flow past three-dimensional orography. *Journal of Fluid Mechanics* 390, 223-249.

Wang, H. F., Y. Zhou and C. K. Chan and K. S. Lam (2006) Effect of initial conditions on interaction between a boundary layer and a wall-mounted finite-length-cylinder wake. *Physics of Fluids* 18,065106.

Wang, H. F. and Y. Zhou (2009). The finite-length square cylinder near wake. *Journal of Fluid Mechanics* 638, 453-490.

Wang, J., W. Zhao, Z. Su and G. Zhang, P. Li and D. Yurchenko (2020). Enhancing vortex-induced vibrations of a cylinder with rod attachments for hydrokinetic power generation. *Mechanical Systems and Signal Processing* 145, 106912.

Wang, M. Y., C. W. Yang, Z. L. Li, S. F. Zhao, Y. F. Zhang and Y. F. Lu (2021). Effects of surface roughness on the aerodynamic performance of a high subsonic compressor airfoil at low Reynolds number. *Chinese Journal of Aeronautics* 34(3), 71-81.

Wille, R. (1974). Generation of oscillatory flows. *Flow-Induced Structural Vibrations*, 1-16.

Yousif, M. Z. and H. Lim (2021). Improved delayed detached-eddy simulation and proper orthogonal decomposition analysis of turbulent wake behind a wall-mounted square cylinder. *AIP Advances* 11(4), 045011.

Zhang, D., L. Cheng and H. An and M. Zhao (2017). Direct numerical simulation of flow around a surface-mounted finite square cylinder at low Reynolds numbers. *Physics of Fluids* 29(4), 045101.